J. Fluid Mech. (2014), *vol.* 754, *pp.* 232–249.
doi:10.1017/jfm.2014.396

The propagation of gravity currents in a V-shaped triangular cross-section channel: experiments and theory

Marius Ungarish[1,†], Catherine A. Mériaux[2] and Cathy B. Kurz-Besson[2]

[1]Department of Computer Science, Technion, Israel Institute of Technology, Haifa 32000, Israel

[2]Instituto Dom Luiz, Faculdade de Ciências, Universidade de Lisboa, Campo Grande 1749-016 Lisboa, Portugal

(Received 20 January 2014; revised 1 June 2014; accepted 7 July 2014; first published online 31 July 2014)

We investigate the motion of high-Reynolds-number gravity currents (GCs) in a horizontal channel of V-shaped cross-section combining lock-exchange experiments and a theoretical model. While all previously published experiments in V-shaped channels were performed with the special configuration of the full-depth lock, we present the first part-depth experiment results. A fixed volume of saline, that was initially of length x_0 and height h_0 in a lock and embedded in water of height H_0 in a long tank, was released from rest and the propagation was recorded over a distance of typically $30x_0$. In all of the tested cases the current displays a slumping stage of constant speed u_N over a significant distance x_S, followed by a self-similar stage up to the distance x_V, where transition to the viscous regime occurs. The new data and insights of this study elucidate the influence of the height ratio $H = H_0/h_0$ and of the initial Reynolds number $Re_0 = (g'h_0)^{1/2}h_0/\nu$, on the motion of the triangular GC; g' and ν are the reduced gravity and kinematic viscosity coefficient, respectively. We demonstrate that the speed of propagation u_N scaled with $(g'h_0)^{1/2}$ increases with H, while x_S decreases with H, and $x_V \sim [Re_0(h_0/x_0)]^{4/9}$. The initial propagation in the triangle is 50 % more rapid than in a standard flat-bottom channel under similar conditions. Comparisons with theoretical predictions show good qualitative agreements and fair quantitative agreement; the major discrepancy is an overpredicted u_N, similar to that observed in the standard flat bottom case.

Key words: geophysical and geological flows, gravity currents

1. Introduction

In its broadest sense, a gravity current (GC) appears when fluid of one density, ρ_c, spreads into a fluid of another density, ρ_a, in a mainly horizontal propagation. GCs occur at a variety of scales throughout nature. Examples include oceanic fronts, avalanches, seafloor turbidity currents, pyroclastic flows, and lava flows. Most studies have focused on the flow of currents which propagate on the flat bottom of a

†Email address for correspondence: unga@cs.technion.ac.il

rectangular channel. If the Reynolds number is large, as assumed here, the lateral boundaries of the rectangular channel are unimportant, and a standard laterally unbounded GC can be assumed (see Simpson 1997; Ungarish 2009). The analytical modelling, experimental, and numerical-simulation tools for the analysis and prediction of currents in rectangular channels are well developed. However, GCs generated and spreading in channels with non-rectangular cross-sections are realistic configurations in nature (e.g. valleys and rivers) and environmental/industrial settings (flow under the roofs of buildings and tunnels, irrigation and drainage systems, oil and gas transport). It is therefore of both practical and academic importance to extend the tools of analysis from the rectangular channel to the counterpart with inclined or curved side-walls, and to assess the quality of the extended models by careful experiments. The present study is concerned with the extension of the thin-layer approximation to the V-shaped valley geometry (shallow-water (SW) theory for the almost-inviscid flow, and lubrication theory for the subsequent viscous flow).

The availability of good approximate models and insights is of higher importance for the non-rectangular case than for the rectangular one. The reasons are as follows. (i) The rectangular current can be simulated fairly well with a 2D xz Navier–Stokes code on moderate grids of roughly 1000×200 intervals (see Bonometti, Balachandar & Magnaudet 2008), in a small number of hours on a laptop computer. Here x means the horizontal direction of propagation, and z the vertical. Such simulations provide efficient verification, and supplementary details, to the predictions of the models. However, a channel with a non-rectangular cross-section requires a 3D simulation because the boundary conditions depend on the lateral coordinate y. The necessary code, and data processing, are more complicated; more importantly, a 3D simulation with a modest 100 grid intervals in the lateral direction takes many CPU hours and large memory space. We argue that the numerical simulation for the non-rectangular channel is expected to be of the same complexity as the simulations of GCs in the presence of bottom bumps or obstacles; see Constantinescu (2014) and Nasr-Azadani & Meiburg (2014). These papers, and the references therein, indicate that computational and data processing efforts is by about two orders of magnitude larger than in 2D simulations. Such large simulation codes and computer resources are certainly not available to many potential users of GCs. Even where available, such a simulation is not a direct competitor to a model that provides the flow-field essentials in several laptop CPU seconds, in spite of the unavoidable approximation errors. (ii) Our 'intuition' is based on rectangular channels, but there is no clear-cut extension to other cases. For example, there is evidence that a current in a V-shaped valley moves faster than on a flat bottom, but our intuition and flat-bottom models cannot explain this observation, nor predict with confidence the stages of the motion and the speed. Actually, can a simple model both qualitatively and quantitatively predict the current velocity and the typical stages of motion in the V-shaped valley? A candidate model is available, as specified later in § 3, and its validation requires benchmarking with laboratory experiments. This validation task is the topic of our paper.

This study is concerned with the class of GCs called either 'compositional-driven' or 'homogeneous'. In the compositional-driven currents, the density difference between the 'current' and the 'ambient' is a result of a dissolved component, for instance, salt in water in lakes and oceans. In the homogeneous currents, the density difference results from a temperature contrast such as cold air in warmer air, or the opposite, in the atmosphere. In such class of currents, the density difference between the current and the ambient remains constant during the propagation, because in many cases

of interest the molecular or thermal diffusion can be neglected during a period of significant propagation.

In the context of our investigation, we note that compositional-driven or homogeneous currents in nature are often propagating while interacting with topography, or landforms. We provide some examples. (i) Based on a Doppler lidar measurement campaign, Gohm *et al.* (2010) described in great detail the passage of a cold front recognized as a density current propagating in the Wipp valley (Austria) in November 1999. Studying the sea breezes in the broad Rhône valley and narrow Durance valley, Bastina *et al.* (2005) noted that lateral constriction of the sea breeze could accelerate the propagation. (ii) Hiscott *et al.* (2013) using various field measurements, demonstrate that the Bosphorus Strait is a large-scale channel network, where saline underflows of GC type interact with the topography. In both of these cases, regardless of the origin of the density contrast (i.e. thermal or compositional), the fundamental flow is that of a high-Reynolds number Boussinesq GC in a channel of non-rectangular cross-section. We therefore argue that a good understanding and modelling of such currents is needed. This also applies to currents on smaller scales, such as the propagation of smoke under the roof of a tunnel, or discharge of cooling fluid in a drainage duct. We emphasize that a significant effect in these flows is the presence of a constraining non-rectangular 'bottom' or 'top' along which the current spreads out. Again, GCs in rectangular or laterally unconstrained channels have been well investigated, but this body of knowledge cannot be applied with confidence and accuracy to the non-rectangular cases. A carefully derived and corroborated set of extensions is needed, and our work attempts to contribute in this direction.

The investigation of the flow field of high-Reynolds-number GCs in channels with non-rectangular cross-sections is a relatively new topic (Marino & Thomas 2009, 2011; Monaghan *et al.* 2009*a*,*b*; Mériaux & Kurz-Besson 2012; Ungarish 2012). The main objective is to determine the speed and shape of the currents, in particular for the typical lock-release problem. The modelling consists mostly of extensions of SW formulations of the type used for the standard rectangular case. In this model the dependent variables are the height of the interface h and the speed u, being averaged over the cross-section area of the current, as functions of time t and horizontal position x. The common features of the currents, irrespective of the shape of the channel, are: the hydrostatic pressure, the propagation of perturbations by waves-characteristics and a jump condition at the nose. Marino & Thomas (2009, 2011) and Ungarish (2012) generalized Benjamin (1968) steady-state analysis. Zemach & Ungarish (2013) have developed a one-layer SW Boussinesq formulation. Ungarish (2013) presented the two-layer SW model, valid for Boussinesq and non-Boussinesq systems. Solutions of these models were presented for various practical cross-sections (power-law, trapezoidal, circular).

The SW models for the standard rectangular geometry have been subjected to numerous supportive verification against both Navier–Stokes simulations and laboratory experiments (for example: Rottman & Simpson 1983; Shin, Dalziel & Linden 2004; Birman, Martin & Meiburg 2005; Lowe, Rottman & Linden 2005; Bonometti, Ungarish & Balachandar 2011; Rotunno *et al.* 2011). In contrast, for the non-rectangular cross-section, there is very little evidential support to the theoretical models. The support must come from Navier–Stokes simulations and laboratory experiments; since the first type of corroboration needs expensive 3D computations and data processing, it seems that, in the near future, the laboratory experiments are a more promising approach for the verification and extension of the theoretical models. This inference was the guiding line of the present work.

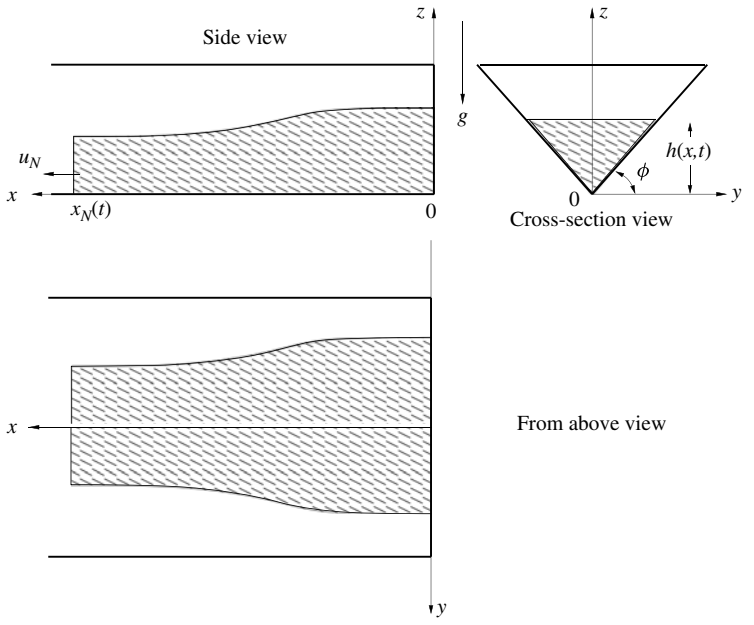

FIGURE 1. Schematic description of the lock-released current in the V-shaped cross-section channel.

Useful experimental data for non-rectangular cross-sections were presented by Marino & Thomas (2009, 2011) and Monaghan *et al.* (2009*b*) for V and power-law shapes. However, the available information covers a very restricted parameter range, as all of the experiments were performed with a full-depth lock at $H = 1$, where H is the initial depth ratio of ambient to current fluids. It is well known that this is a very special configuration, in which a backward-moving bore appears in the lock, and is then reflected from the backwall. The models predict that H is an important dimensionless governing parameter in the behaviour of the current, therefore a reliable comparison between theory and experiment must be over a range of H. Furthermore, the experiments of Marino & Thomas (2009, 2011) were concerned mostly with the speed of propagation during the slumping stage; and while Monaghan *et al.* (2009*b*) observed also the later stages of propagation, the details of the transition between stages were not under focus. We believe that a reliable verification of the positions where the slumping stage ends, and where viscous influence begins, is important for the modelling and understanding of the GC.

The present work attempts to close some of the previously mentioned gaps of knowledge. We focused attention on the motion of saline GCs in a V-shaped triangular channel, see figure 1. We performed experiments for both full- and part-depth locks. In particular, we analysed the extent of the various stages of propagation, and compared our experimental results to the theoretical predictions. Our conclusion is that the available models are useful and consistent extensions of the counterparts in the standard rectangular geometry.

The present paper is devoted to the compositional-driven, or homogeneous, currents. A different class of currents is named 'particle-driven' because in these flows the density difference with the 'ambient' is due to suspended particles in the 'current'. Examples are turbidity currents, in which sediments are suspended in sea water,

or pyroclastic flows in which solid fragments, known as tephras, are suspended in hot gas. In contrast to the compositional-driven or homogeneous currents, the density difference in particle-driven currents is decreasing during the propagation as sedimentation occurs. Therefore the SW study of such currents is more difficult, and it is more effectively performed after a good understanding of the simpler, homogeneous current, has been developed (see, for example, Bonnecaze, Huppert & Lister 1993; Hogg, Ungarish & Huppert 2000). Like the homogeneous currents, particle-driven currents in non-rectangular cross-section channels also have numerous interesting geophysical and environmental applications such as submarine surges produced by earthquakes and landslides, erosion of rivers (see Simpson 1997; Kneller & Buckee 2000). However, there are strong practical reasons for not combining the classes of homogeneous and particle-driven currents into one investigation. While this work is concerned with the experimental corroboration of the theoretical modelling of the various phases of motion of the homogeneous current in both partial- and full-depth configurations, no counterpart model for the particle-driven currents exists, and no partial-depth particulate currents are experimentally feasible as there is no practical way particles could be maintained in suspension until the system is set up for the current's release. For the particle-driven current in a V-shaped triangular cross-section at full-depth lock release, a 'box model' has been presented and calibrated by experimental data by Monaghan *et al.* (2009*a*) and Mériaux & Kurz-Besson (2012). The box model is a simplification, and cannot predict correctly the slumping stage, and influence of the part-depth lock, which were under focus in the present investigation. Moreover, particle-driven currents display physical effects such as sedimentation and particle run-out that have no counterpart in the homogeneous current; this means that special experimental measurements and data processing are needed. These considerations lead to the conclusion that the most efficient method of investigation is to deal first with the homogeneous current, and then use the knowledge and insights to extend the work to the particle-driven counterpart in a future study. We wish to mention that this was also the order in the rectangular case: the SW models for the particle-driven flow (Bonnecaze *et al.* 1993; Hogg *et al.* 2000) were based on, and include, the extensive knowledge acquired for homogeneous currents (Benjamin 1968; Huppert & Simpson 1980; Rottman & Simpson 1983).

The structure of the paper is as follows. The laboratory experiments are described in § 2. The theoretical model used for comparisons is presented briefly in § 3. In § 4 we analyse the experimental data, with emphasis on the slumping speed u_N and slumping distance x_S dependencies on H, and the distance x_V of transition to viscous regime dependency on the Reynolds number. In § 5 some concluding remarks are given. A short derivation of the theoretical distance x_V is given in appendix A.

2. The laboratory experiments

The lock-exchange experiments were carried out in a Perspex rectangular tank 5 m long and 30 cm wide, in which had been inserted a channel of triangular cross-section, see figure 2. The channel of triangular cross-section had a height H_0 of 6.65 cm. Two fluids, that were water and an aqueous solution, were used. The current consisted of the saline fluid of density ρ_c, while the ambient fluid was the less dense water, of density ρ_a. At the start of each experiment, the gate of the lock was placed at a distance $x_0 = 13$ cm from one end of the tank, referred to as the 'backwall'. The lock and the rest of the tank were then filled at the same rate. The height of the dense

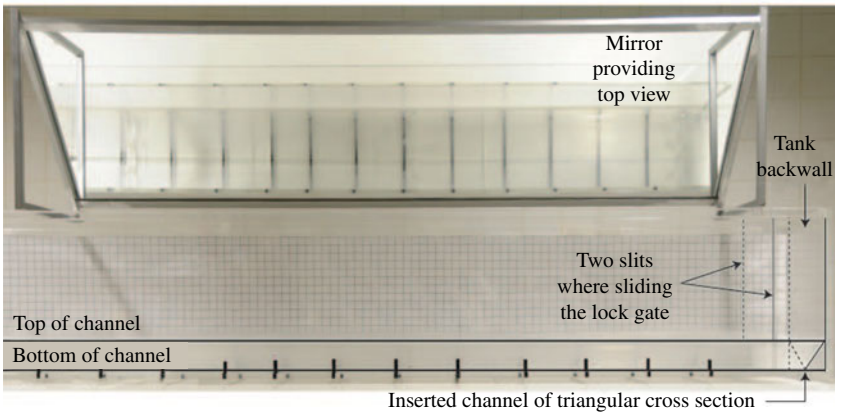

FIGURE 2. Experimental tank. The photo is only showing the first 2.5 m of the tank.

fluid in the lock is denoted by h_0. In the full-depth experiments, the lock and the rest of the tank, separated by the gate, were filled up to the same depth, $h_0 = H_0$, with the saline solution and water, respectively. In the partial-depth experiments, the lock and the rest of the channel were first filled up to a height h_0 with the saline solution and water, respectively. Fresh water was subsequently very carefully added on both sides of the lock gate to the total depth H_0. The lock had then a clearly defined horizontal density interface between the saline solution and water before the gate was rapidly lifted to release the dense fluid, which typically took 0.24 s.

The saline solution was dyed to provide flow visualization. Each experiment was recorded by a video camera. The motion of the current was monitored over 5 m = $38.5x_0$ length, by recording the time t_i at which the front reached marked x_i positions in the tank. There were 19 marks, at smaller intervals for the first half of the tank near the lock, and larger in the second half (where deceleration was expected).

We performed seven experiments, whose main parameters are presented in table 1. The height of the ambient fluid $H_0 = 6.5$ cm, and the lock length $x_0 = 13$ cm, were constant in all of the experiments. The height of the saline in the lock, h_0, varied. The depth ratio $H = H_0/h_0$ ranged from 1.00 to 2.15; two of the experiments were of full-depth release type, $H = 1$. The lock aspect ratio, x_0/h_0, changed from 2 to 4.2 as H increases from 1 to 2.15. The initial density difference was approximately 9 % in five experiments; two of these experiments, with $H = 1$ and 1.51, were also repeated for a density difference close to 5 %. The initial Reynolds numbers, Re_0, are also given in table 1. The large values of this parameter (>5000) indicate that all of the tested currents were expected to be in the inertial-buoyancy regime for a significant distance of propagation of several lock lengths. The large value of this parameter also implies a very large Péclet number ($=\kappa Re_0$, because the Schmidt number κ is approximately 700 for saline). There were no heat sources inside or close to the experimental fluids, and the heat generated during the gate removal process, and the internal dissipation of the moving fluids, could produce only insignificant gradients of temperature in the flow field. Consequently, the molecular mass diffusion effects, and heat transfer, were negligible during the recorded time of propagation of the current.

A video for experiment 7 PD, showing the typical time-dependent evolution of the flow is given in the online supplementary material available at http://dx.doi.org/10.1017/jfm.2014.396.

https://doi.org/10.1017/jfm.2014.396 Published online by Cambridge University Press

Experiment number and type	$(\rho_c - \rho_a)/\rho_c$ (%)	h_0 (cm)	g'_0 (cm s^{-2})	H	Re_0	x_0/h_0	U (cm s^{-1})	T (s)
1 FD	4.8	6.65	47	1.00	11 788	2.0	17.73	0.733
2 FD	9.2	6.65	91	1.00	16 327	2.0	24.55	0.530
3 PD	9.2	6.00	91	1.11	14 011	2.2	23.35	0.557
4 PD	9.0	5.00	89	1.33	10 544	2.6	21.09	0.616
5 PD	4.9	4.40	48	1.51	6 398	3.0	14.54	0.894
6 PD	9.2	4.40	91	1.51	8 799	3.0	19.92	0.653
7 PD	9.1	3.10	89	2.15	5 160	4.2	16.65	0.781

TABLE 1. Experimental conditions. Full-depth and partial-depth experiments are referred as FD and PD, respectively. Here $g' = (1 - \rho_a/\rho_c)g$, where g is the gravitational acceleration. Here $U = \sqrt{g'h_0}$, $T = x_0/U$ are the scaling speed and time, respectively. Here $Re_0 = Uh_0/\nu$, where the kinematic viscosity of water ν is 10^{-2} cm^2 s^{-1}.

3. Theoretical model

3.1. *Scaling*

It is convenient to introduce the density ratio parameter R of light to heavy fluids, and the reduced gravity

$$R = \frac{\rho_a}{\rho_c}; \quad g' = \frac{\rho_c - \rho_a}{\rho_c} g = (1-R)g, \tag{3.1a,b}$$

where g is the gravitational acceleration. The scaling speed U and time T are as in the classical case,

$$U = (g' h_0)^{1/2}; \quad T = x_0/U. \tag{3.2a,b}$$

The x lengths are scaled by x_0, the vertical z lengths (heights) and the lateral y lengths are scaled by h_0.

The dimensionless parameters of our problem are: the height ratio of ambient to lock H; the density ratio R; the lock aspect ratio x_0/h_0; and the initial Reynolds number, defined as $Re_0 = Uh_0/\nu$, where $\nu = 0.01$ cm^2 s^{-1}. The shape of the cross-section is a triangle that is symmetric about the xz plane, see figure 1. The angle of the sidewalls with horizontal is $\phi = 25°$.

The $H = 1$ case is referred to as 'full-depth lock', and the initial stage as lock exchange; the other cases, as part depth.

3.2. *Theoretical model predictions*

If the initial Reynolds number Re_0 is large, the propagation after the release at $t = 0$ is in the buoyancy-inertia inviscid regime. The SW approximation provides the governing equations for the position of the interface h measured from the bottom line of the tank, see figure 1, and the area-averaged velocity u of the dense fluid, as functions of t, x (see Ungarish 2013 for details). Let $a = a(x,t) = h/H$. For the present triangular cross-section current, the continuity and momentum equations are

$$\begin{cases} \dfrac{\partial h}{\partial t} + u\dfrac{\partial h}{\partial x} + \dfrac{h}{2}\dfrac{\partial u}{\partial x} = 0, \\ \dfrac{\partial u}{\partial t} + D\dfrac{\partial h}{\partial x} + (1-2B)u\dfrac{\partial u}{\partial x} = 0, \end{cases} \tag{3.3}$$

where

$$B = \frac{Ra^2}{1-a^2}(1-a^2+Ra^2)^{-1} \quad \text{and} \quad D = \left[1 - a^2 - R\left(\frac{1}{1-a^2}\right)^2 \frac{2}{H} a u^2\right](1-a^2+Ra^2)^{-1}. \tag{3.4a,b}$$

The partial differential equation system (3.3) is hyperbolic, with characteristic relationships and trajectories given by

$$\frac{\mathrm{d}h}{\mathrm{d}u} = \frac{1}{D}\left[Bu \mp \sqrt{(Bu)^2 + D\frac{h}{2}}\right], \quad \text{on } \frac{\mathrm{d}x}{\mathrm{d}t} = c_\pm = u(1-B) \pm \sqrt{(Bu)^2 + D\frac{h}{2}}. \tag{3.5}$$

The initial/boundary conditions are $h = 1$, $u = 0$ in the lock at $t = 0$, and $u = 0$ at the backwall $x = 0$. The nose, denoted by subscript N, is treated as a jump of

height h_N. At $x = x_N(t)$, we apply the extension of Benjamin's (1968) result to the present geometry (Marino & Thomas 2009, 2011; Ungarish 2012):

$$u_N = \frac{1}{R^{1/2}} Fr(h_N/H)\ h_N^{1/2}; \quad Fr(a) = \left[2\frac{(1-a^2)}{1+a^2}\left(1-\frac{1}{3}a^2\right)\right]^{1/2}. \tag{3.6a,b}$$

We emphasize that the inviscid SW model is for a general 'apex-down' triangle of width bz, $(0 \leqslant z \leqslant H,\ b > 0)$. The angle of inclination of the side walls is relevant to the viscous regime, see below.

The Boussinesq case is obtained by setting $R = 1$ in the governing equations. Another simplification, for deep ambient ($H > 2$, roughly), is the one-layer SW model, which discards the return flow in the ambient. This is obtained by setting $D = 1, B = 0$ in the governing equations (see Marino & Thomas 2009, 2011; Monaghan *et al.* 2009*b*; Zemach & Ungarish 2013).

The SW model is self-contained and does not use adjustable constants. The analysis and solution are performed by reliable mathematical tools: the method of characteristics, similarity techniques and finite-difference codes. Some general insights for the triangular cross-section can be derived. The theory predicts that there is an initial 'slumping' stage of propagation with constant u_N, over a significant distance x_S, which decreases with H. The slumping u_N can be obtained analytically, as shown in Ungarish (2013) and Zemach & Ungarish (2013). For large t, the SW theory predicts the analytical self-similar solution with $x_N(t) = 1.694\ t^{4/5}$ (Monaghan *et al.* 2009*b*; Zemach & Ungarish 2013). In this stage the speed, thickness and the typical inertia u_N^2/x_N decay significantly with t. The current becomes prone to viscous influence.

The SW model becomes invalid after the current spreads to a distance x_V, where the viscous forces become influential. The analysis presented in appendix A gives for the present geometry

$$x_V = 0.32[Re_0 h_0/x_0]^{4/9}. \tag{3.7}$$

Note that the power 4/9 does not depend on the apex angle of the triangle, but the coefficient 0.32 does.

We keep in mind that the model is based on simplifications. Diffusion of heat and components (say salt), neglected in the model, occur in real systems over finite time scales. An order of magnitude analysis demonstrates that the influence of these effects is like $1/(\kappa Re_0)$; the Schmidt or Prandtl numbers κ are approximately 1 or more in many cases of interest (κRe_0 is also defined as the Péclet number). Therefore, high-Reynolds-number GCs usually pertain to large-Péclet-number flows, and hence it is justified to neglect the influence of mass diffusion and heat transfer on the propagation of the current for $x < x_V$ at least. In addition, the interface of a real current develops local eddies and instabilities, and the head of the current is affected by turbulence and entrainment. In this context we must rely on studies performed for rectangular currents (Hallworth *et al.* 1996; Johnson & Hogg 2013) which demonstrate that these effects have little influence on the speed of propagation for a significant length of spread of the current. In view of these considerations, there are good reasons to expect that the model provides a good approximate description of the GC phenomenon, in the sense that it reveals the salient features of the flow, points out the governing dimensionless parameters, predicts the trend of influence of these parameters, provides fairly accurate values of the speed of propagation and its qualitative changes with time, and provides an estimate for the range of validity. The answer to the question whether, and how well, these expectations are fulfilled brings us to the following section.

x_i	t_i (1 FD)	t_i (2 FD)	t_i (3 PD)	t_i (4 PD)	t_i (5 PD)	t_i (6 PD)	t_i (7 PD)
1.00	0.00	0.00	0.00	0.00	0.00	0.00	0.00
2.38	2.35	1.89	2.21	2.22	2.07	2.35	2.15
3.68	4.25	3.81	4.04	4.10	3.56	4.08	4.33
4.98	6.30	6.01	6.14	5.99	5.95	6.12	5.57
6.18	8.19	7.89	7.90	7.66	7.44	7.94	7.76
7.68	10.27	10.42	10.31	10.06	9.54	9.51	9.86
9.00	12.31	12.28	12.16	12.21	11.55	11.81	12.04
10.31	14.60	14.79	14.42	13.30	13.78	14.35	14.58
11.54	16.65	16.98	16.58	15.75	15.77	15.58	17.32
12.60	18.28	18.56	18.41	17.36	18.01	17.92	20.12
13.91	20.56	20.77	20.80	20.36	20.56	20.23	24.23
15.32	22.91	23.29	22.58	22.76	23.86	23.10	29.09
16.63	25.40	24.87	25.60	25.18	27.31	26.89	34.79
19.50	30.31	30.39	31.35	33.12	37.46	34.16	52.71
23.10	39.57	38.30	40.11	42.56	53.70	48.38	87.57
26.93	50.68	49.08	51.07	59.14	82.87	69.88	147.35
30.77	66.83	60.77	64.97	82.97	132.65	104.99	248.49
34.62	87.82	75.62	85.25	117.83	222.38	159.87	424.32
37.94	113.65	92.97	106.92	161.52	335.03	237.12	665.23

TABLE 2. Dimensionless experimental propagation measurements.

4. Analysis of experimental data

The preliminary observations are as follows. The experiments are concerned with dense bottom GCs in a channel of V-shape, or ∇, triangular cross-section (to be distinguished from the Λ-shaped, or Δ, triangular cross-section). The density difference, $1 - R$, is approximately 5 or 10 %; this can be considered in the Boussinesq domain. The initial Reynolds number is large in all tested cases ($5 \times 10^3 < Re_0 < 16 \times 10^3$), and hence the currents are in the buoyancy-inertial regime over a significant distance of propagation.

We performed the analysis in dimensionless form, using the scaling introduced in the previous section. The recorded propagation $x_N(t)$ is summarized in table 2, and figure 3 shows the collapse of the dimensionless data on a log–log plot. The dimensionless length of the channel is 38.5.

In all of the experiments, we observed an initial propagation with $u_N = \text{const}$. This motion, called the slumping stage, lasts over a significant distance that is at least five lock-lengths from the gate. The slopes $\mathrm{d}x_N/\mathrm{d}t$ during the slumping and the slumping distance differ according to the dimensionless height H. After the slumping phase, the current decelerates.

For GCs of fixed volume released from behind a lock, as in the present case, the major comparison between theory and experiment is concerned with the slumping u_N. We first note a qualitative agreement: the SW theory predicts that the initial propagation is with constant speed, and the experiments confirm this prediction, for all of the tested cases. The novelty is that here the confirmation is for various H; to the best of the authors' knowledge, the existence of the slumping stage was confirmed before only for the full-depth release (Marino & Thomas 2009, 2011; Monaghan *et al.* 2009*b*).

The quantitative comparison of the slumping speed u_N is shown in figure 4. We estimated the experimental u_N by line fit to sections of $x_N(t)$, and finite differences.

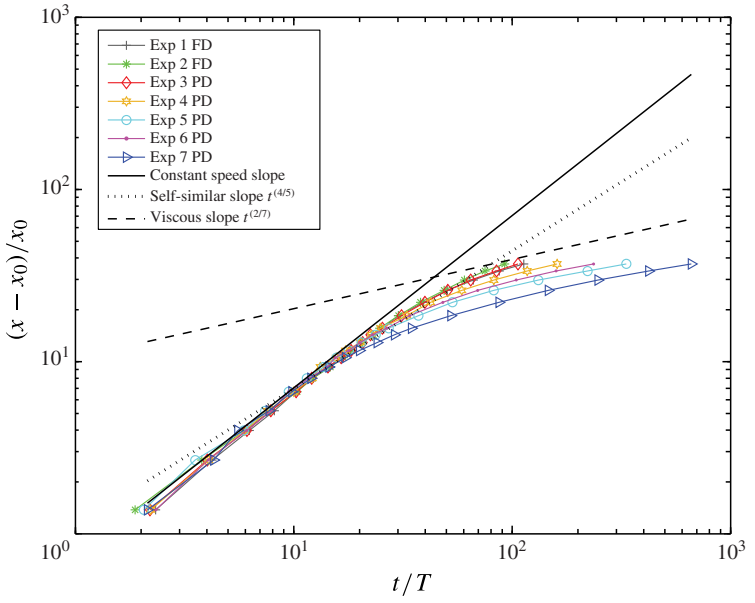

FIGURE 3. (Colour online) Log–log plot of dimensionless experimental distance of propagation (measured from gate) versus dimensionless t, scaled according to § 3.1. The three stages of propagation can be seen.

Overall, the error of the experimental u_N reported here is approximately $\pm 5\,\%$. As most of our experiments are for $H < 2$, a significant return flow is expected in the ambient. Consequently, for our theoretical predictions we used the two-layer SW model.

The theory predicts an increase of u_N with H; the experiments confirm this prediction. However, the measured points are, consistently, below the SW prediction. The discrepancy is, typically, 20 %. We nevertheless claim that the experimental results provide validation to the extension of the SW theory for the triangular cross-section.

We argue that the observed compatibility between the theoretical predictions and measurements is actually the best agreement that can be expected between the SW theory and laboratory experiments with currents over a solid bottom. Our reference is the classical rectangular counterpart. There is ample evidence that in a rectangular cross-section channel, the SW two-layer theory produces exactly the same agreement–discrepancy pattern when compared with the experiments; see Rottman & Simpson (1983), Shin *et al.* (2004) and Lowe *et al.* (2005). Consider a specific case: for $H = 1$, $R = 0.953$, the SW prediction is $u_N = 0.54$ while the experimental value of Lowe *et al.* (2005) is $u_N = 0.42$ (i.e. $-22\,\%$ discrepancy). In our case, the SW prediction is 0.77 while the experimental value is 0.63 (i.e. $-18\,\%$ discrepancy). In other words, the change of geometry from rectangle to triangle increases both the experimental and the theoretical values by approximately 50 %; however, in both cases the experiment is approximately 20 % below the theory. The same trend was detected for the range of H covered by our experiment. We conclude that the SW theory for the triangular cross-section provides the same accuracy as in the classical rectangular case.

This brings us to other related questions: (i) what is the reason for this discrepancy; (ii) what is the value of the SW theory if the predicted speed disagrees 20 % with

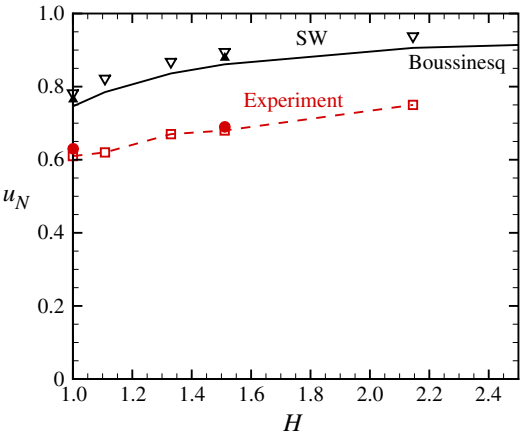

FIGURE 4. (Colour online) The experimental and theoretical u_N during slumping, as function of H. The symbols are experimental results: square for $R = 0.908$ and circle for $R = 0.951$. The solid line shows the SW Boussinesq theory; the nearby Δ and ∇ symbols show SW non-Boussinesq results for $R = 0.908, 0.952$, respectively.

experiments; and (iii) is there a practical remedy? For the rectangular cross-section we answer as follows. (i) Navier–Stokes simulations with free-slip conditions on the horizontal boundaries of the channel produce GCs whose u_N is in good agreement with the SW predictions (Birman *et al.* 2005; Rotunno *et al.* 2011). This seems to indicate that the friction at the bottom, not accounted for in the SW theory, is the main reason for speed reduction. (ii) The SW models are a valuable tool for general predictions and insights. In spite of efforts over several decades, there is no other self-contained theory for the high-Reynolds-number GC, which predicts correctly the slumping stage, transition to self-similar stage, and the influence of the governing parameters in both the Boussinesq and non-Boussinesq domains. Here we see that the SW formulation also predicts correctly the effect of non-rectangular cross-section. (iii) The observation that the experimental u_N is consistently below the SW predictions by approximately 20 %, provides a useful indication about the necessary correction in practical applications. Moreover, the use of a semi-empirical Fr formula, such as that suggested by Huppert & Simpson (1980) rather than the theoretical Benjamin's result improves the agreement with laboratory measurements. We expect that these answers are also relevant to non-rectangular cross-sections, but the analysis is beyond our objectives and means. We keep in mind that for our geometry: no Navier–Stokes simulations are available, neither non-Boussinesq data, and nor a Fr formula of the Huppert–Simpson type for use in (3.6). The acquirement of this knowledge requires substantial additional work which must be left for the future.

4.1. *End of slumping, self-similar and transition to viscous regime*

The SW model predicts that, at some distance x_S, the Boussinesq current begins to decelerate, and eventually enters into a stage of self-similar propagation of the form $x_N = 1.694t^{4/5}$. The theory also predicts that x_S decreases when H increases. At the removal of the gate, a backward wave propagates into the lock; then is reflected from the backwall $x = 0$ to the nose. Until this wave reaches the nose, the current propagates with the initial slumping speed u_N. The theoretical waves-characteristics propagate faster for larger H. Hence, x_S becomes shorter when H increases.

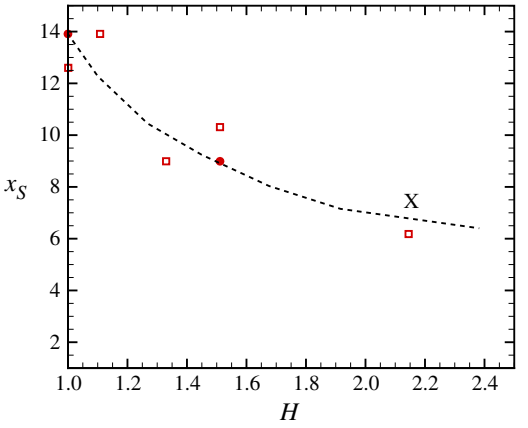

FIGURE 5. (Colour online) End of slumping x_S as function of H. The symbols are experimental results for $R = 0.908$ (squares) and $R = 0.951$ (circles). The X is the SW one-layer Boussinesq model prediction. The dashed line is a free-hand pattern.

Figure 5 presents the experimental results for the distance x_S as a function of H. There is overall agreement with the theoretical expectation and interpretation. We must keep in mind that this is not a sharply defined variable. The position where deceleration starts is, at best, determined within the resolution of the interval between the measurement points, whose dimensionless value is approximately 1.3. In any case, it is quite clear that x_S decreases significantly (from 14 to 6) as H increased from 1 to 2.15.

The exact calculation of x_S by the two-layer SW theory requires a sophisticated calculation which is beyond our objective. However, for $H = 2.15$, the one-layer SW theory is a good approximation, and we inserted the corresponding predicted value in the figure ($x_S = 7.4$, symbol X).

Theoretically, for $x \gg x_S$ the inertial-buoyancy current attains self-similar propagation $x_N \sim t^{4/5}$. The log–log plot of the experimental x_N versus t, see figure 3 reveals the 4/5 slope, but for only a relatively short distance of propagation. This is because in our tests the Reynolds numbers are not excessively large, and hence viscous effects begin to decelerate the $\sim t^{4/5}$ propagation at a quite moderate distance, x_V. Roughly, $x_V - x_S$ is less than 10, so that the current can barely develop the self-similar motion before the viscous influence appears.

The distance of transition to the viscous regime, x_V, is shown in figure 6. We define x_V as the position where the inertia dominance ends, because the viscous friction at the bottom becomes significant. A fully developed viscous current propagates like $t^{2/7}$ according to an exact solution of the thin-layer viscous equations developed by Takagi & Huppert (2007). We observed the tendency to this pattern in the log–log $x_N(t)$ plot of the experiments (figure 3). However, the inertia-buoyancy regime ends at the theoretical 'point' where the power of t, or slope on log–log $x_N(t)$ plot, changes from the self-similar 4/5 toward 2/7; this position is not sharp, as shown in figure 3.

The theoretical trend $x_V = C[Re_0 h_0/x_0]^{4/9}$ is in good agreement with the experimental observations. This estimate under-predicts the experimental position of transition by approximately 5 units, i.e. lock lengths. The discrepancy of x_V between theory and experiment can be attributed to both theoretical and experimental reasons. The theoretical estimate is based on the overlap of two self-similar solutions of the form

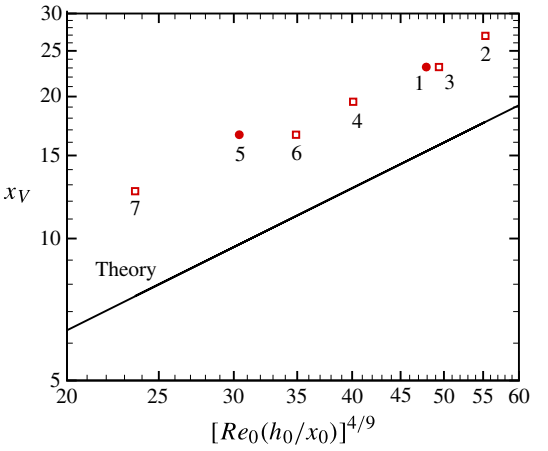

FIGURE 6. (Colour online) Transition to a viscous regime, x_V as function of $[Re_0(h_0/x_0)]^{4/9}$ (log–log axes). The symbols are the experiments (with corresponding numbers). The line is the theoretical (A 6).

$x_N = K_j t^{\beta_j}$, where j represents the inertial and viscous regimes. However, it is well known that these are asymptotic formulas for t and $x_N \to \infty$. Actually, the time t in these formulas admits a 'virtual origin' shift, which is negligible only after very long propagation. Here the asymptotic formula is used for non-large values of t and x_N and, hence, the accuracy of the theoretical x_V is low. In the experiments, the detection of x_V is not sharp. However, in spite of this ambiguity, the data indicate a consistent larger-than-predicted x_V for all of the experiments. This suggests that the main reason for discrepancy is the theoretical estimate, not the experimental error.

4.2. *Motion in the lock*

The SW theory predicts that after the removal of the gate a wave propagates into the lock, and is then reflected from the backwall. In particular, for the full-depth $H = 1$ case, this is a bore of speed 0.39 and amplitude 0.21 (scaled with h_0). In our experiments the lock domain was inspected from above, but not many details could be discerned. In the experiment 2 FD ($H = 1$) a sharp disturbance was seen to propagate from the gate to the backwall, in 1.5 s, i.e. the backward dimensionless speed is 0.36. This is in fair agreement with the prediction; however, we could not measure the amplitude of this wave. After reflection, this wave could no longer be observed from above. We realized that a more detailed study of the return flow requires a longer lock, but this could not be performed in the available apparatus.

5. Concluding remarks

We investigated, mostly by experimental means, the motion of high-Reynolds-number homogeneous, or compositionally-driven, GCs in a horizontal channel with a V-shaped triangular cross-section. The novelty is that we systematically considered: (i) the influence of the height-ratio parameter, H; (ii) the slumping distance x_S, over which the speed of propagation u_N is constant; and (iii) the distance x_V where transition to the viscous regime occurs. We emphasize that the theoretical models used in this work contain no adjustable parameters.

In general, the experiments are consistent with the predictions of the available theoretical models for this type of geometry, but there are some quantitative discrepancies. The experiments confirm the existence of the slumping stage with constant u_N for all H, the increase of u_N with increasing H, and the decrease of x_S with increasing H. The experiments confirm that the inertia-buoyancy (inviscid) propagation is restricted to a spread of about $[Re_0(h_0/x_0)]^{4/9}$, after which transition occurs to the viscous regime studied by Takagi & Huppert (2007). The experimental slumping speed is consistently below the SW theory prediction, by approximately 20 %. However, we emphasize that this is exactly the accuracy obtained in the counterpart standard rectangular-cross-section problem. For a given H, the measured slumping speed, scaled with $(g'h_0)^{1/2}$, is larger by approximately 50 % in the triangle than in the rectangle, in accord with the SW predictions. We therefore claim that the extension of the theory from the standard to the more complicated cross-section cases seems to be successful, and it makes sense to use it and invest in its further testing and development.

We are aware of the fact that realistic GCs in nature and environmental/industrial circumstances might contain various effects such as interfacial turbulence, mixing and entrainment; diffusion and heat transfer between the current and ambient fluids. These effects are expected to be negligible for the range of parameters of and flow-field variables focused on in the present investigation; moreover, the filtering out of these small-scale mechanisms renders a more clear-cut insight into the fundamental governing equations and backbone mechanisms. A solution of the flow field which takes into account these effects requires careful numerical simulations. Since the non-rectangular cross-section geometry needs a 3D code, these simulations will request many CPU hours on powerful computers. To the best of the authors' knowledge, no such simulations have been performed or are underway although the state of the art seems ripe for such computations, see Constantinescu (2014) and Nasr-Azadani & Meiburg (2014). On the other hand, the simplified SW model provides some essential features of the flow field in insignificant CPU time on a standard laptop computer. Therefore, in spite of its limitations, the model is, in our opinion, a useful platform for practical estimates, and further research progress. The model and its present corroborations against experiments are also expected to be useful in the debugging and validation process of the future Navier–Stokes simulation tools. In these contexts, an interesting extension of the SW model and of the present experiments would be to the class of particle-driven currents; the works of Bonnecaze *et al.* (1993), Hogg *et al.* (2000), Monaghan *et al.* (2009*a*) and Mériaux & Kurz-Besson (2012) are expected to provide helpful insights. Another extension of practical use will be the incorporation of entrainment effects; here the recent paper of Johnson & Hogg (2013) provides promising guiding lines.

Finally, we note that in a Boussinesq system a 'top' (light) current under a Λ-shaped roof is the mirror image of the 'bottom' (heavy) current in a V-shaped valley. All our present results carry over to the light current counterpart upon the change that the boundary $z=0$ on which propagation occurs is the top, the coordinate z and the height (thickness) h are measured downward, and $g'=|1-\rho_a/\rho_c|g$.

Acknowledgements

Both C.M. and C.B. are funded by the Ciências 2009 programme of the Fundaçao para a Ciência e a Tecnologia (FCT, Portugal). The present work was supported by FCT under Project Pest-OE/CTE /LA0019/2013–2014.

Supplementary movie

Supplementary movie is available at http://dx.doi.org/10.1017/jfm.2014.396.

Appendix A. Theoretical estimate of the distance of viscous transition x_V

Let x_V be the distance at which the current changes regime from inertial to viscous. Suppose that in both regimes a similarity solution is relevant, so that

$$x_N(t) = K_j t^{\beta_j}, \tag{A 1}$$

where $j = I$ for inertial and $j = V$ for viscous, and the values of K_j and β_j are known. The speed of propagation is

$$u_N = \dot{x}_N = \beta_j K_j t^{\beta_j - 1} = \beta_j K_j^{1/\beta_j} x_N^{1-1/\beta_j}, \tag{A 2}$$

where the $t = (x_N/K)^{1/\beta}$ relationship was used. The variables are scaled as specified in § 3.1.

If Re_0 is sufficiently large (as in our experiments) the regime transition occurs after the slumping stage is finished, and the current has entered into the inertial self-similar stage. Thus, the transition from inertial to viscous regimes is between two self-similar forms. We argue that the transition is smooth and, hence, at this occurrence, both regimes display the same speed of propagation. We therefore write, for the transition

$$\beta_I K_I^{1/\beta_I} x_N^{1-1/\beta_I} = \beta_V K_V^{1/\beta_V} x_N^{1-1/\beta_V}. \tag{A 3}$$

The value of x_N which satisfies this equation is the transition x_V. We obtain the explicit result

$$x_V = \left[\beta_V K_V^{1/\beta_V} / \beta_I K_I^{1/\beta_I}\right]^q; \quad q = \beta_V \beta_I / (\beta_I - \beta_V). \tag{A 4}$$

We note in passing that the result (A 4) is valid and useful for various cross-section geometries, provided that K_j, β_j are known. Here, for the V-shaped triangle, we use the solutions of Takagi & Huppert (2007) and Zemach & Ungarish (2013) for the inertial and viscous regimes, respectively. This provides $\beta_I = 4/5$, $\beta_V = 2/7$, $K_I = 1.694$, and

$$K_V = 1.768[PRe_0 h_0/x_0]^{2/7}, \tag{A 5}$$

where $m = \cot(\phi)$, $P = 0.137m^2/[2(1+m^2)]$. Here ϕ is the angle of the bottom with the horizontal; see figure 1. Substitution into (A 4) and some algebra yield

$$x_V = C(m)[Re_0 h_0/x_0]^{4/9}, \tag{A 6}$$

where $Re_0 = (g' h_0)^{1/2} h_0/\nu$. Here $C = 1.15P^{4/9}$ depends on ϕ. In our experiments, $\phi = 25°$, $C = 0.32$.

For a standard rectangular cross-section the estimated transition form inertial to viscous regimes is given by $x_V = C_1[Re_0 h_0/x_0]^{2/7}$, where C_1 is a constant of order unity (see Ungarish (2009, Section 2.7) and the references therein). It is interesting to note that in both cases the relevant Reynolds number is actually $Re_0 h_0/x_0$. It is also interesting, perhaps even surprising, that the power 4/9 for the triangular case does not depend on the apex angle. The power of $Re_0 h_0/x_0$ is smaller in the rectangular case than in the triangular, which implies a shorter x_V for a given Re_0. This is surprising, because the impression is that the triangle provides more friction than the typically wide rectangle. The justification is geometric: in the triangle the height

(average thickness) of the current of fixed volume decreases like $1/x_N^{1/2}$, while in a rectangle the thickness is like $1/x_N$. Since the speed of propagation, and the inertia, are proportional to the thickness, we infer that the rectangular current losses its inertia against the viscous shear sooner than a triangular current. When the inclination angle ϕ increases x_V decreases, as could be expected because, for a given volume, the contact with the sidewalls is enhanced. In the limit $\phi \to 90°$, $C(m)$ and x_V decrease to zero, because the current is confined in a thin wedge. On the other hand, for $\phi \to 0$ the value $C(m)$ is 0.35; the rectangular case x_V is not recovered, because even in this limit, the current is assumed to be confined in a triangular, wide-wedge, cross-section.

REFERENCES

BASTINA, S., DROBINSKIA, P., DABASB, A., DELVILLEC, P., REITEBUCHD, O. & WERNER, C. 2005 Impact of the Rhone and Durance valleys on sea-breeze circulation in the Marseille area. *Atmos. Res.* **74**, 303–328.

BENJAMIN, T. B. 1968 Gravity currents and related phenomena. *J. Fluid Mech.* **31**, 209–248.

BIRMAN, V. K., MARTIN, J. E. & MEIBURG, E. 2005 The non-Boussinesq lock exchange problem. Part 2: high-resolution simulations. *J. Fluid Mech.* **537**, 125–144.

BONNECAZE, R. T., HUPPERT, H. E. & LISTER, J. R. 1993 Particle-driven gravity currents. *J. Fluid Mech.* **250**, 339–369.

BONOMETTI, T., BALACHANDAR, S. & MAGNAUDET, J. 2008 Wall effects in non-Boussinesq density currents. *J. Fluid Mech.* **616**, 445–475.

BONOMETTI, T., UNGARISH, M. & BALACHANDAR, S. 2011 A numerical investigation of constant-volume non-Boussinesq gravity currents in deep ambient. *J. Fluid Mech.* **673**, 574–602.

CONSTANTINESCU, G. 2014 Les of lock-exchange compositional gravity currents: a brief review of some recent results. *Environ. Fluid Mech.* **14**, 295–317.

GOHM, A., MAYR, G. J., DARBY, L. S. & BANTA, R. M. 2010 Evolution and structure of a cold front in an Alpine valley as revealed by a Doppler lidar. *Q. J. R. Meteorol. Soc.* **136**, 962–977.

HALLWORTH, M., HUPPERT, H. E., PHILLIPS, J. & SPARKS, R. 1996 Entrainment into two-dimensional and axisymmetric turbulent gravity currents. *J. Fluid Mech.* **308**, 289–311.

HISCOTT, R. N., AKSU, A. E., FLOOD, R. D., KOSTYLEV, V. & YASAR, D. 2013 Widespread overspill from a saline density-current channel and its interaction with topography on the south–west Black Sea shelf. *Sedimentology* **60**, 1639–1667.

HOGG, A., UNGARISH, M. & HUPPERT, H. E. 2000 Particle-driven gravity currents: asymptotic and box-model solutions. *Eur. J. Mech. (*B*/Fluids)* **19**, 139–165.

HUPPERT, H. E. & SIMPSON, J. E. 1980 The slumping of gravity currents. *J. Fluid Mech.* **99**, 785–799.

JOHNSON, C. G. & HOGG, A. J. 2013 Entraining gravity currents. *J. Fluid Mech.* **731**, 477–508.

KNELLER, B. & BUCKEE, C. 2000 The structure and fluid mechanics of turbidity currents: a review of some recent studies and their geological implications. *Sedimentology* **47**, 62–94.

LOWE, R. J., ROTTMAN, J. W. & LINDEN, P. F. 2005 The non-Boussinesq lock exchange problem. Part 1: theory and experiments. *J. Fluid Mech.* **537**, 101–124.

MARINO, B. M. & THOMAS, L. P. 2009 Front condition for gravity currents in channels of nonrectangular symmetric cross-section shapes. *Trans. ASME J. Fluids Engng* **131** (5), 051201.

MARINO, B. M. & THOMAS, L. P. 2011 Dam-break release of a gravity current in a power-law channel section. *J. Phys.: Conf. Ser.* **296**, 012008.

MÉRIAUX, C. A. & KURZ-BESSON, C. B. 2012 Sedimentation from binary suspensions in a turbulent gravity current along a V-shaped valley. *J. Fluid Mech.* **712**, 624–645.

MONAGHAN, J., MÉRIAUX, C., HUPPERT, H. & MANSOUR, J. 2009*a* Particulate gravity currents along V-shaped valleys. *J. Fluid Mech.* **631**, 419–440.

MONAGHAN, J., MÉRIAUX, C., HUPPERT, H. & MONAGHAN, J. 2009*b* High Reynolds number gravity currents along V-shaped valleys. *Eur. J. Mech. (*B*/Fluids)* **28** (5), 651–659.

NASR-AZADANI, M. M. & MEIBURG, E. 2014 Turbidity currents interacting with three-dimensional seaflor topography. *J. Fluid Mech.* **745**, 409–443.

ROTTMAN, J. & SIMPSON, J. 1983 Gravity currents produced by instantaneous release of a heavy fluid in a rectangular channel. *J. Fluid Mech.* **135**, 95–110.

ROTUNNO, R., KLEMP, J. B., BRYAN, G. H. & MURAKI, D. J. 2011 Models of non-Boussinesq lock-exchange flow. *J. Fluid Mech.* **675**, 1–26.

SHIN, J. O., DALZIEL, S. B. & LINDEN, P. F. 2004 Gravity currents produced by lock exchange. *J. Fluid Mech.* **521**, 1–34.

SIMPSON, J. E. 1997 *Gravity Currents in the Environment and the Laboratory*. Cambridge University Press.

TAKAGI, D. & HUPPERT, H. E. 2007 The effect of confining boundaries on viscous gravity currents. *J. Fluid Mech.* **577**, 495–505.

UNGARISH, M. 2009 *An Introduction to Gravity Currents and Intrusions*. Chapman & Hall/CRC Press.

UNGARISH, M. 2012 A general solution of Benjamin-type gravity current in a channel of non-rectangular cross-section. *Environ. Fluid Mech.* **12** (3), 251–263.

UNGARISH, M. 2013 Two-layer shallow-water dam-break solutions for gravity currents in non-rectangular cross-area channels. *J. Fluid Mech.* **732**, 537–570.

ZEMACH, T. & UNGARISH, M. 2013 Gravity currents in non-rectangular cross-section channels: analytical and numerical solutions of the one-layer shallow-water model for high-Reynolds-number propagation. *Phys. Fluids* **25**, 026601.